Geophysical Research Letters

RESEARCH LETTER
10.1029/2019GL084838

Parathethys Last Gasp in Central Asia and Late Oligocene Accelerated Uplift of the Pamirs

Xin Wang[1], Barbara Carrapa[2], James B. Chapman[3], Susana Henriquez[2], Mi Wang[1], Peter G. DeCelles[2], Zaijun Li[1], Fei Wang[1], Ilhomjon Oimuhammadzoda[4], Mustafo Gadoev[4], and Fahu Chen[1,5]

[1]Key Laboratory of Western China's Environmental Systems (Ministry of Education), College of Earth and Environmental Sciences, Lanzhou University, Lanzhou, China, [2]Department of Geosciences, University of Arizona, Tucson, AZ, USA, [3]Department of Geology and Geophysics, University of Wyoming, Laramie, WY, USA, [4]Institute of Geology, Earthquake Engineering and Seismology of the Academy of Sciences, Dushanbe, Tajikistan, [5]Key Laboratory of Alpine Ecology, CAS Center for Excellence in Tibetan Plateau Earth Sciences and Institute of Tibetan Plateau Research, Chinese Academy of Sciences (CAS), Beijing, China

Abstract Cenozoic sedimentary rocks in the Tajik Basin record the history of retreat of the Paratethys from central Asia, tectonic activity within the surrounding Pamir and Tian Shan mountains, and Asian aridification. However, there remains a paucity of precise chronological constraints on the sequences from this region. Here we present integrated magnetostratigraphic, detrital zircon and monazite U-Pb geochronologic, and detrital apatite fission track thermochronologic data from the lower Cenozoic sedimentary sequences in the Tajik Basin. Our results indicate that the investigated sedimentary rocks were deposited between ~41 and 23.3 Ma, with a depositional hiatus between ~36 and 31 Ma. The last two marine regressions were dated at ~41 and ~37.4 Ma, respectively. Eolian sandy loess dominates the sequences from ~31 to ~25 Ma and gradually transitions to fluvial facies after ~25 Ma, consistent with late Oligocene to early Miocene acceleration of active deformation, uplift, and exhumation of the Pamirs.

Plain Language Summary Central Asia has experienced prolonged climatic changes, from a relatively hot and humid climate, influenced by the Paratethys, to an extremely dry continental climate, during the Cenozoic. Precise chronological constraints on the sedimentary sequences that record this transition are required for resolving the forcing mechanisms behind this significant paleoclimate change. We report a reliable chronological framework for the lower Cenozoic sedimentary record in the Tajik Basin, which was occupied by the Paratethys during the early Cenozoic and a foreland basin related to uplift of the Pamir-Tian Shan orogen. Our new data help advance scientific understanding of the sea retreat, mountain building, and long-term climate changes in central Asia during the early Cenozoic.

Key Points:
- We report the first high-resolution magnetostratigraphy of sedimentary sequences in the Tajik Basin spanning from ~23.3 to ~41 Ma
- The penultimate and ultimate retreat of the Paratethys from central Asia were dated at ~41 and ~37.4 Ma, respectively
- The Pamir Mountains have experienced active deformation and accelerated exhumation during the late Oligocene to early Miocene (~25 Ma)

Supporting Information:
- Supporting Information S1
- Table S1
- Table S2
- Table S3

Correspondence to:
X. Wang,
xinw@lzu.edu.cn

Citation:
Wang, X., Carrapa, B., Chapman, J. B., Henriquez, S., Wang, M., DeCelles, P. G., et al. (2019). Parathethys last gasp in central Asia and late Oligocene accelerated uplift of the Pamirs. *Geophysical Research Letters*, *46*. https://doi.org/10.1029/2019GL084838

Received 2 AUG 2019
Accepted 25 SEP 2019
Accepted article online 15 OCT 2019

1. Introduction

The retreat of the Paratethys from central Asia (e.g., Bosboom et al., 2017; Popov et al., 2004) and the stepwise uplift of the Tibetan-Pamir Plateau (e.g., Kapp & DeCelles, 2019; Tapponnier et al., 2001; Yin, 2010) are the most significant midlatitude geological events in central Asia during the Cenozoic. This land-sea reorganization (e.g., Meijer et al., 2019; Ramstein et al., 1997) and/or mountain building event (e.g., Liu et al., 2015; Molnar et al., 2010) drove long-term climatic changes in central Asia, resulting in the formation of the largest extratropic arid zone on Earth. However, there remains substantial debate on the timing, processes, and mechanisms responsible for these geological and paleoclimatic events.

Previous chronological and paleoclimatic studies have mainly focused on Cenozoic sedimentary sequences in the southwestern Tarim Basin, east of the Pamir Plateau. Magnetostratigraphic and paleontological work indicates that the ultimate retreat of the Paratethys from the Tarim Basin occurred during the late Eocene (e.g., Bosboom et al., 2014, 2017; Sun et al., 2016; Sun & Jiang, 2013; Wang et al., 2014, 2016; Yang et al., 2015). Low-temperature thermochronologic and sedimentological work revealed episodic erosional and tectonic activity of the Pamir-Tian Shan mountains in the Cenozoic (e.g., Sobel & Dumitru, 1997; Coutand et al., 2002; Robinson et al., 2007; Carrapa et al., 2014; Cao et al., 2014, Cao et al., 2015; Blayney et al., 2016; Rutte et al., 2017; Liu et al., 2017); however, the timing and amplitude of the uplift events associated with these

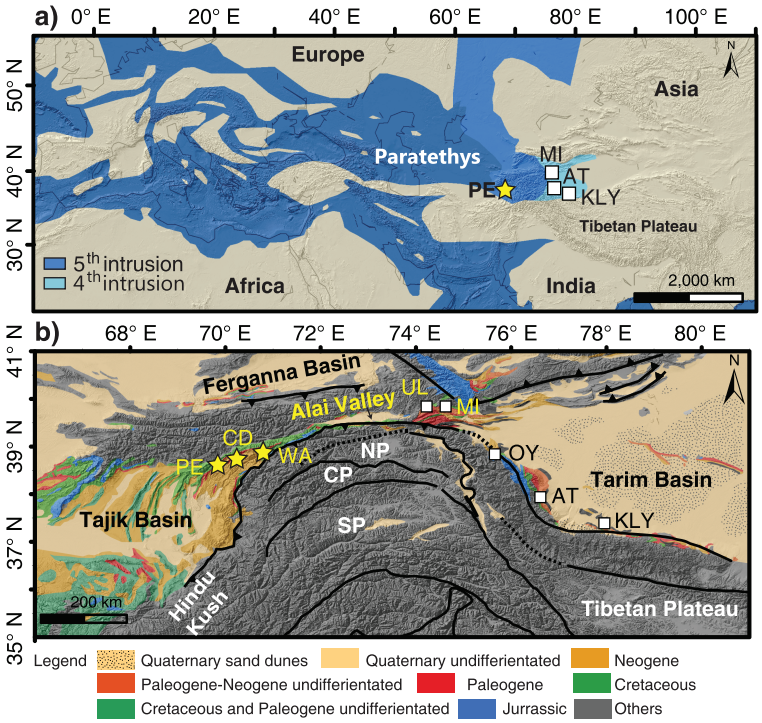

Figure 1. Map showing the location and geological setting of the study region. (a) Paleogeographic maps showing the land-sea distribution in Euro-Asia during the late Eocene (after Wang et al., 2014). (b) Simplified geologic map of the study area (after Wang et al., 2016). The yellow star indicates the working sections, and the white square indicates sections included for comparison. Abbreviations: UL = Ulugqat (Wang et al., 2014); MI = Mine (Yang et al., 2015); OY = Oytag (Sun & Jiang, 2013); AT = Aertashi (Bosboom et al., 2014; Zheng et al., 2015); KLY = Keliyang (Sun et al., 2016); NP = northern Pamir; CP = central Pamir; SP = southern Pamir.

records remain controversial. To fully understand Cenozoic paleogeographic and paleoclimate changes over central Asia, additional data are required from west of the Pamirs.

The Tajik Basin was covered by the Paratethys sea during the early Cenozoic and is a flexural foreland basin related to the uplift of the Pamir-Tian Shan orogen (Figure 1; Carrapa et al., 2015; Chapman et al., 2017). The Pamir formed as a result of accretion of allochthonous terranes to Eurasia during the Mesozoic and experienced significant crustal thickening and uplift since the late Eocene (Burtman & Molnar, 1993; Carrapa et al., 2015; Chapman et al., 2019). The Tian Shan is part of a Paleozoic orogenic system that was reactivated during the late Cenozoic (Sobel & Dumitru, 1997; Worthington et al., 2017). Paleogene strata in the Tajik Basin are characterized by alternating shallow-marine and continental redbed deposits, which can be correlated with those from the southwestern Tarim Basin, and record the last three (third to fifth) transgressive-regressive cycles of the Paratethys over central Asia (Bosboom et al., 2017; Carrapa et al., 2015; Kaya et al., 2019; Klocke et al., 2017; Sun et al., 2016; Wang et al., 2014, 2016). The Neogene sequences in the Tajik Basin are dominated by syntectonic clastic deposits with high temporal and spatial variability in facies, thickness, and composition (Klocke et al., 2017; Chapman et al., 2019; Figure S1 and Table S1 in the supporting information). These sedimentary sequences provide ideal archives for reconstructing the geographic and climatic changes in central Asia during the Cenozoic.

We present new paleomagnetic, detrital zircon and monazite geochronology, and detrital apatite fission track (AFT) thermochronology data from the Peshtova (PE, 38°36.093′N, 69°55.325′E), the Childara (CD, 38°46.607′N, 70°18.350′E), and the west Algurkan (WA, 38°50.805′N, 70°51.380′E) sections in the northeastern Tajik Basin (Figure 1). By integrating our results with previously published zircon U-Pb geochronology (Carrapa et al., 2015) and paleomagnetic data from the lower part of the PE section (Wang et al., 2016), we have established the first high-resolution magnetostratigraphic framework for the lower to middle Cenozoic sedimentary sequences in the Tajik Basin. This provides a reliable chronological framework for understanding the timing of sea retreat, mountain building, and paleoclimate changes in central Asia.

2. Materials and Methods

2.1. Magnetostratigraphy Method

Oriented core samples were collected from well-exposed siltstone and fine-grained sandstone layers using a portable drill. Oriented block samples were collected from friable mudstone layers that are not easily drilled. Stratigraphic intervals composed of carbonate rocks, coarse-grained sandstone, and poorly exposed intervals were avoided for sampling. A total of 878, 271 and 41 oriented paleomagnetic samples were collected from the PE, CD, and WA sections, respectively.

In order to investigate the main magnetic carriers, we selected 10 representative samples for rock magnetism analysis on a variable field transition balance at Fujian Normal University and three pilot samples for high-temperature, low-field susceptibility experiments using a KLY-2 Kappabridge susceptibility meter at the University of Utah. All the samples were cut into 2-cm cubes/diameter specimens for further analyses. In a magnetically shielded (<300 nT) room, the natural remanent magnetizations (NRMs) were measured, and then, each specimen was progressively demagnetized in an MMTD80 thermal demagnetizer using up to 14 temperature steps with intervals of 100 °C up to 250 °C, 50 °C from 250 to 400 °C, and 40 °C from 400 to 680 °C. NRMs were measured after each demagnetization step using a 2G 760R Superconducting Rock Magnetometer at the Key Laboratory of Western China's Environmental Systems, Lanzhou University.

2.2. AFT Thermochronology Method

AFT analyses were performed on three detrital (sandstone) samples using the external detector method (Tagami et al., 1987). More than 100 detrital apatite grains were targeted per sample and mounted in epoxy resin and polished for dating. The mounts were etched in 5.5-M nitric acid for 20 s at 21 °C before irradiation. The irradiation was performed at Oregon State University. After irradiation, mica external detectors were etched in 40% hydrofluoric acid for 45 min at 21 °C. Analyses were conducted for optical identification of fission tracks using an Olympus microscope at 1,600X magnification with a drawing tube located above a digitizing tablet and a Kinetek computer-controlled stage driven by the FT Stage program. The fission track analyses were performed at the Fission Track Laboratory in the University of Arizona. Additional analytical information can be found in Table S2.

2.3. U-Pb Geochronology Method

Three detrital (sandstone) samples were collected from the PE section (PE1680, PE1625, and PE825) for U-Pb geochronology. Zircon and monazite grains were extracted from rock samples by traditional mineral separation methods, mounted in epoxy, polished to expose the interior of the crystals, and imaged using backscatter electron and cathodoluminescence imaging at the University of Arizona LaserChron scanning electron microscope facility. Both zircon and monazite geochronology were conducted at the University of Arizona LaserChron Center following standard procedures (Gehrels et al., 2008). U-Pb geochronology of zircons was conducted by laser ablation single-collector inductively coupled plasma mass spectrometry. Approximately 300 zircon grains were measured from each sample. Analysis of monazite was performed using a Photon Machines 193-nm excimer laser coupled to a Nu Instruments high-resolution multicollector inductively coupled plasma mass spectrometry. Analyses were conducted with a 10-μm-diameter laser spot using an acquisition routine similar to zircon U-Pb analyses. The primary monazite standard was 44069 (Aleinikoff et al., 2006), and the secondary standard was 554 (Harrison et al., 1999). Additional analytical information can be found in Tables S3 and S4.

3. Results

3.1. Rock Magnetism Results

Pilot samples from the PE, CD, and WA sections yield relatively lower saturation magnetization, lower saturation remanence, and higher coercive force (Figure S2a), indicating the presence of magnetically hard materials such as hematite (Tauxe, 2009). The curie/Néel temperature is around 670 °C (Figure S2a), suggesting that the main magnetic carrier is hematite. High-temperature, low-field susceptibility results (Figure S2c) and the normalized NRM decay curves (Figure S2d) further suggest that the main magnetic carrier in most samples is hematite. Specifically, hysteresis loops of one sample from the Miocene strata from the PE section are narrow at the center and closed around 300 mT (Figure S2b). Thermomagnetic curves of this sample have

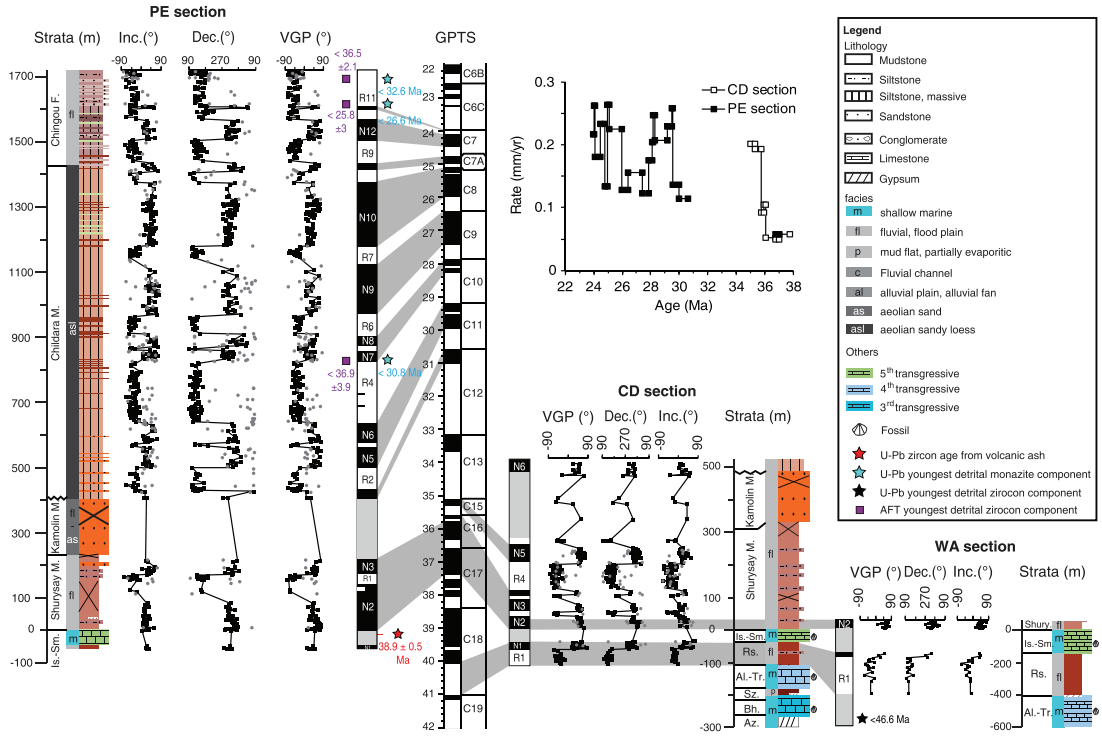

Figure 2. Chronology of the Lower Cenozoic sedimentary sequences in the Tajik Basin. The U-Pb age of volcanic ash in the lower part of the PE section and sedimentary facies are from Carrapa et al. (2015). The paleomagnetic data for the lower PE section (0- to 500-m interval) are from Wang et al. (2016). The datum for the stratigraphic column is defined as the top of the stratigraphically highest shallow marine strata for comparison purposes. Abbreviations for formation/member name: Az. = Akdzha; Bh. = Bukhara; Sz. = Suzak; Al. = Alai; Tr. = Turkestan; Rs. = Rishtan; Is. = Isfara; Sm. = Sumsar; Shury. = Shurysay.

a major drop in magnetization near 580 °C and followed a small progressive decrease until 680 °C (Figure S2b), indicating the presence of dominant magnetite and minor hematite (Tauxe, 2009).

3.2. Demagnetization Stabilities and Tests

The demagnetization can be subdivided into three groups according to the differences in stability. Group 1 generally has stable demagnetization behavior. On the orthogonal vector plots, these samples generally yield two components (Figure S3a). The first one is unblocked at low temperatures generally ranging from 0 to 300 °C, which is interpreted as a secondary thermoviscous remanent magnetization component. The second component shows that relatively stable directions and the vectors decay toward the origin and is interpreted as the characteristic NRM (ChRM) component. A principal component analysis of least squares fit (Kirschvink, 1980) was used to calculate the mean direction of the second component (at least four successive thermal steps), and the stabilities were evaluated by the maximum angular deviations (MADs). Samples from this group have MAD < 15°. Group 2 yields stable demagnetization behaviors and have MAD < 15°. However, their ChRM declination and inclination values were not consistent in terms of normal or reversed polarity or the virtual geomagnetic pole latitudes of these ChRM directions are >45° larger than the mean values from those of the Group 1 samples (Figure S3b). These data were eliminated from the final magnetostratigraphic determination (Deenen et al., 2011). Nevertheless, the 45° cutoff data were plotted as discrete gray cycles on the polarities to provide a complete magnetostratigraphic framework (Figures 2 and S4). Group 3 is characterized by highly irregular demagnetization behaviors along with the increased heating temperatures, which has MAD > 15° (Figure S3c). These samples mainly consist of coarse-grained sandstone samples and thus were rejected for further analyses.

Magnetostratigraphy of each section can be established based on the data with best qualities (Group 1, Table S5). The paleomagnetic polarity are defined by the virtual geomagnetic pole calculated from the ChRM declination and inclination data. On our polarity subdivisions, the shortest polarity event is defined by at least three ChRM directions of good quality (Figure 2). Finally, 447, 140, and 36 reliable ChRM directions were

obtained from the PE, CD, and WA sections, respectively. After tilt correction, the mean normal and reversed directions are close to be antipodal (Figures S4a–S4c), which passes the C quality reversal test (McFadden & McElhinny, 1990). Paleomagnetic samples in the lower part (−55- to 217-m interval) and upper part (409–1,722 m) of the PE section were collected from the north and south limbs of an anticline, respectively (Figure S5). The mean directions of reversed and normal intervals from the two limbs are scattered in the in situ (geographic) coordinate system, but coherence significantly improved after adjusting for tilt (Figure S4d). This provides evidence for a pretilt acquisition of remanence (Tauxe, 2009). In addition, magnetostratigraphic records from the PE, CD, and WA sections are comparable (Figure 2), suggesting that the ChRMs obtained in this study are primary NRMs.

3.3. Magnetostratigraphy and Correlations

The magnetostratigraphic results from the Rishtan Fm. are consistent between the CD and WA sections (Figure 2); they are characterized by a long reversal interval (R1 from the CD and WA sections) in the lower part of the section and short normal interval (N1 from the CD and WA sections) in the upper part. U-Pb dating of detrital zircon grains from underlying shallow marine portion of the WA section suggests that the continental redbeds of the Rishtan Fm. are younger than ~46.6 Ma (Carrapa et al., 2015). Zircon U-Pb dating of a volcanic ash from shallow marine strata overlying the redbeds indicates that they are older than ~38.9 ± 0.5 Ma (Carrapa et al., 2015). By using independent zircon U-Pb geochronology and paleontology (Bosboom et al., 2017) age constraints, the Rishtan Fm. best correlates with C18 of the geomagnetic polarity time scale (GPTS) 2016 (Ogg et al., 2016), which results in a basal and upper age of ~41 and ~ 40 Ma for the ~100-m-thick continental redbeds between the two shallow marine intervals (Figure 2).

The magnetostratigraphy of the Shurysay member in the CD section consists of four pairs of normal (N2–N5) and reversed (R2–R5) intervals and is characterized by two long normal events (N2 and N3) intercalated with a stable reversed event (R1) in the PE section (Figure 2). The thick covered layer in the PE section (80- to 120-m interval) resulted in uncertainties in the polarity determinations. Magnetostratigraphy of the Shurysay member in the CD section is more reliable and can be correlated with C17–C15 of the GPTS 2016 (Figure 2). This preferred correlation suggests that the age of the base of the Shurysay member is ~37.4 Ma, consistent with the U-Pb age of the volcanic ash from the PE section (Carrapa et al., 2015) and with paleontological data from the Eocene strata in the Tajik and the southwestern Tarim basins (Bosboom et al., 2017; Kaya et al., 2019).

The Kamolin member is not suitable for paleomagnetic study, because of the coarse grain size and limited ferromagnetic grains. The magnetostratigraphy of the Childara member and the Chingou Fm. in the PE section yielded two strikingly long reversed intervals (R4 and R11) and two long normal intervals (N9 and N10). The two long normal intervals are intercalated with a short stable reversal interval that can be confidently correlated to the C8 and C9 chrons of the GPTS 2016. By using the C8 and C9 chrons as correlation markers, the polarity of the upper section is correlated to the C6C to C11 of GPTS 2016 (Figure 2). This correlation is further confirmed by the youngest detrital monazite age and youngest population of detrital AFT ages (see details below).

It should be noted that no reliable paleomagnetic records were obtained from the Kamolin member, due to the coarse-grained nature of the samples containing limited ferromagnetic minerals that can record the Earth's magnetic field. It is unlikely that the >200-m-thick sandstone was continuously deposited between ~35.2 and 31 Ma, which results in an extremely low depositional rate (i.e., ~0.06 mm/year). Field investigations show abrupt changes in lithology from the top of the Kamolin member and the base of the Childara member (Figure S5), suggesting a regional depositional hiatus. This upper Eocene to lower Oligocene sedimentary hiatus is also found in the Cenozoic sedimentary sequences throughout the western Tarim Basin (Bosboom et al., 2014; Yang et al., 2015) and the eastern Tajik Basin (Chapman et al., 2019).

Under this preferred magnetostratigraphic framework, the average sediment accumulation rates for the Shurysay member, the Childara member of the Baldshuan Fm., and the Chigou Fm. are 0.11, 0.18, and 0.22 mm/year, respectively (Figure 2), yielding an overall increasing trend upsection.

3.4. Detrital Zircon U-Pb and AFT Results

Detrital zircon U-Pb data from the early Cenozoic terrestrial sedimentary rocks in the Tajik Basin exhibit several age populations that range from the pre-Cambrian to the early Cenozoic (Figure 3a and Table S3). Age spectra for the three samples reported in this paper and the two samples reported in Carrapa et al. (2015) are

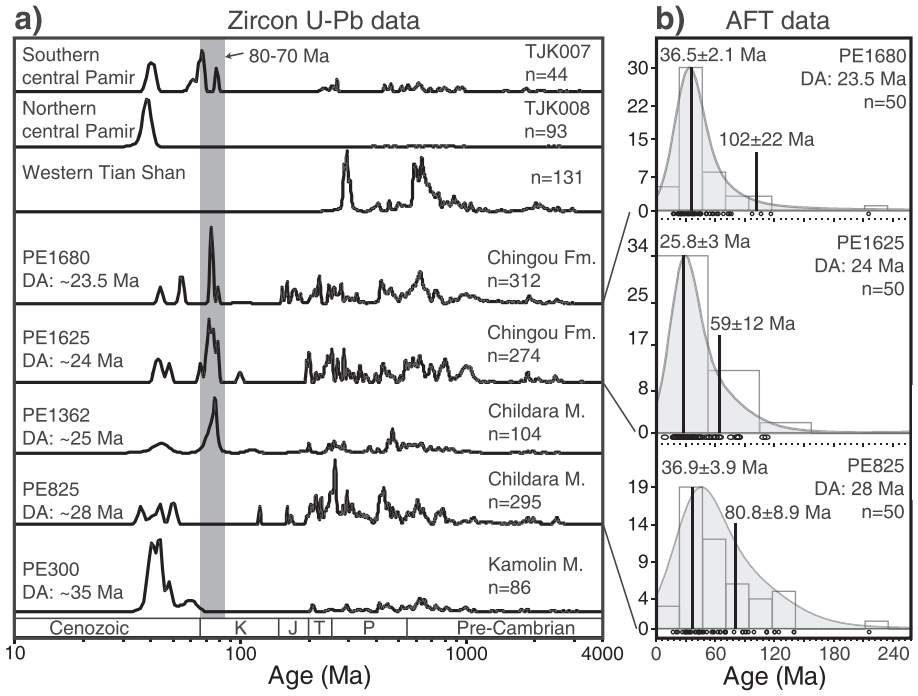

Figure 3. Zircon U-Pb and apatite fission track (AFT) data from the PE section. (a) Normalized kernel density plots for U-Pb detrital zircon data and its comparison with modern detrital sediments sourced from the western Tian Shan (Worthington et al., 2017) and northern and southern Central Pamir terranes (Carrapa et al., 2014; Chapman et al., 2018). The data for PE300 and PE 1362 are from Carrapa et al. (2015). The gray bar indicates the Late Cretaceous (~80–70 Ma) age population observed from the igneous rocks in the southern Central Pamir terrane (Chapman et al., 2018). (b) Density plot and histogram of AFT cooling ages for three samples from the PE section. Density plots made using the software DensityPlotter (Vermeesch, 2012). Note that the youngest age group (approximately 25.8 ± 3 Ma) in PE1625 is, within error, equivalent to the depositional age (DA).

broadly similar to one another but differ in detail. The ~40-Ma age population is the youngest age group for all samples. The Cretaceous age (~80–70 Ma) population is absent in Lower Eocene and Upper Oligocene samples; however, it is present in Upper Oligocene to Lower Miocene samples (Figure 3a). Monazite U-Pb geochronology for three sandstone samples from 825, 1,625, and 1,680 m in the PE section have minimum age populations of 30.8 ± 0.8, 26.7 ± 0.6, and 32.6 ± 0.9 Ma, respectively (Figure 2 and Table S4).

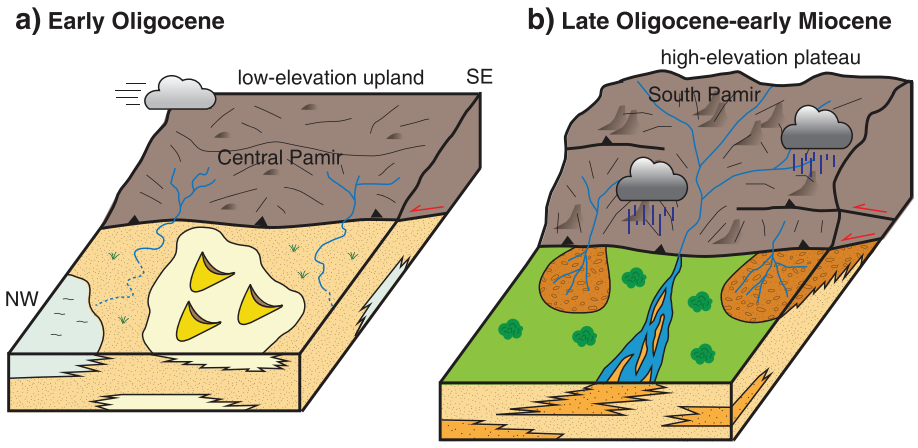

Figure 4. Schematic models showing the depositional environments in the Tajik Basin during the Oligocene to early Miocene.

Three samples from the Tajik Basin were analyzed for detrital AFT thermochronology and display prominent Cretaceous to Cenozoic age populations (Figure 3b). Sample PE1680 from Lower Miocene strata, with a depositional age (DA) of ~23.5 Ma, has age populations of 36.5 ± 32.1 and 102 ± 22 Ma. Sample PE1625 from Lower Miocene strata (DA: ~24 Ma) has age populations of 25.8 ± 3 and 59 ± 12 Ma. Sample PE825 from Lower Oligocene strata (DA: ~28 Ma) has a young age population of 36.9 ± 3.9 Ma and an older age population of 80.8 ± 8.9 Ma (Figure 3b).

4. Summary and Discussions

Geochronological constraints are key for reconstructing Cenozoic paleo-environmental changes over central Asia and for better understanding of its potential linkages between the retreat of the Paratethys, the uplift of the Tibetan-Pamir Plateau, and global climate change. Sufficient sampling resolution, coherence of magnetostratigraphic patterns among three parallel sections, and the unique absolute dating tie points (Carrapa et al., 2015) provide a reliable paleomagnetic framework for lower Cenozoic sedimentary rocks in the Tajik Basin. Our magnetostratigraphic dating suggests that the penultimate (fourth) and ultimate (fifth) retreat of the Paratethys from the Tajik Basin occurred at ~41 and ~37.4 Ma, respectively. The penultimate retreat in the Tajik Basin corresponds to the ~41-Ma retreat event reported from the Mine (MI, Kaya et al., 2019), Aertashi (AT, Bosboom et al., 2014), and Keliyang (KLY, Sun et al., 2016) sections in the southern Tarim Basin (Figure 1). After the fourth regression, the eastern edge of the Paratethys withdrew to a location west of the Tajik Basin. At ~40 Ma, the inland sea advanced and its eastern coastline was located east of the Mine section in the western Tarim Basin (Figure 1; Wang et al., 2014; Bosboom et al., 2017; Kaya et al., 2019). At ~37.4 Ma, the Paratethys retreated from central Asia permanently. Because the ages for the last two regressions are significantly older than major global sea level falls at the Eocene-Oligocene transition but correlate with active tectonics in the Pamir and foreland basin deposition (Carrapa et al., 2015; Chapman et al., 2019), we suggest that regional tectonism played a more important role than global sea level changes in driving the final retreat of the Paratethys from central Asia.

After the final retreat of the Paratethys, arid, eolian depositional environments were common during the late Eocene and were dominated by deposition of sandy loess during the Oligocene (Figure 4a; Carrapa et al., 2015; Wang et al., 2016). Our paleomagnetic dating results help constrain the initiation of eolian sand accumulation to ~37 Ma and indicate that eolian deposition occurred predominantly between ~31 and ~25 Ma. The sedimentary record suggests that a desert-like environment was established in the Tajik Basin during most of Oligocene, corresponding to the establishment of the Antarctic ice sheet and a global cooling period (Zachos et al., 2001).

During the late Oligocene to early Miocene (~25 Ma), sedimentary facies relationships indicate that the depositional environment changed from eolian to fluvial (Figure 4b). Detrital zircon U-Pb age spectra from Upper Oligocene to Lower Miocene sandstone in the Tajik Basin contain ~80- to 70-Ma age populations, which are not present in older strata (Figure 3a), and can only have been derived from Late Cretaceous (approximately 80–70 Ma) igneous rocks located in Central and South Pamir terranes (Chapman et al., 2018). The appearance of the ~80- to 70-Ma age population in Upper Oligocene to Lower Miocene strata in the Tajik Basin suggests that sediment started being supplied from areas located deep within the interior of the Pamir Mountains during this time (Figure 4). This pattern is comparable to provenance changes observed in the southwestern Tarim Basin from the eastern side of the Pamirs (Blayney et al., 2016). We interpret this change in sediment provenance to reflect continued uplift and erosion of the Pamir Mountains (Cao et al., 2015; Jiang et al., 2013; Zheng et al., 2015).

Our youngest detrital AFT population of 25.8 ± 3 Ma from Lower Miocene strata (DA: ~24 Ma) in the Tajik Basin (Figure 3b) suggests a lag time close to 0, which requires very rapid erosion and sediment transport, consistent with an actively exhuming and relatively high-relief sediment source region (i.e., the Pamirs). Thermochronological data from modern river sands show asymmetric exhumation of the Pamirs, which has been interpreted as the result of relatively high topography and orographic effects (Carrapa et al., 2014). Data from the Tajik Basin show the presence of a regional foreland basin with increasing subsidence in the late Oligocene-early Miocene, consistent with topographic load/uplift and increased erosion at this

time (Chapman et al., 2019). This independent evidence coupled with our new AFT data suggests that the Pamirs were actively deforming, uplifting, and exhuming during the late Oligocene-early Miocene (approximately ~25 Ma) and acted as an important barrier to precipitation.

Acknowledgments
We thank Dr. D. H. Sun and J. S. Nie for fruitful discussion, Dr. P. Lippert for assistant in rock magnetism analysis, and two reviewers for constructive comments. Financial support for this research was provided by the National Natural Science Foundation of China (Grant 41672158), the second Tibetan Plateau Scientific Expedition and Research Program (STEP; Grant 2019QZKK0602), the Chinese 111 Project (Grant BP2018001), National Science Foundation (grant EAR-1450917), and the Fundamental Research Funds for the Central Universities (Grant lzyjbky-2019-99). The authors declare no conflict of interest. The data for the work in this paper can be downloaded from the figshare website (https://figshare.com/s/7d26f042b7fec3a1096e) and are available in Tables S2–S5 in the supporting information. Supplementary figures can be found in the supporting information.

References

Aleinikoff, J. N., Schenck, W. S., Plank, M. O., Srogi, L. A., Fanning, C. M., & Kamo, S. L. (2006). Deciphering igneous and metamorphic events in high-grade rocks of the Wilmington complex, Delaware: Morphology, cathodoluminescence and backscattered electron zoning, and SHRIMP U-Pb geochronology of zircon and monazite. *Geological Society of America Bulletin*, *118*(1-2), 39–64. https://doi.org/10.1130/B25659.1

Blayney, T., Najman, Y., Dupont-Nivet, G., Carter, A., Millar, I., Garzanti, E., et al. (2016). Indentation of the Pamirs with respect to the northern margin of Tibet: Constraints from the Tarim basin sedimentary record. *Tectonics*, *35*, 2345–2369. https://doi.org/10.1002/2016TC004222

Bosboom, R., Dupont-Nivet, G., Grothe, A., Brinkhuis, H., Villa, G., Mandic, O., et al. (2014). Linking Tarim Basin sea retreat (west China) and Asian aridification in the late Eocene. *Basin Research*, *26*(5), 621–640. https://doi.org/10.1111/bre.12054

Bosboom, R., Mandic, O., Dupont-Nivet, G., Proust, J., Ormukov, C., & Aminov, J. (2017). Late Eocene palaeogeography of the proto-Paratethys Sea in Central Asia (NW China, southern Kyrgyzstan and SW Tajikistan). *Geological Society, London, Special Publications*, *427*(1), 565–588. https://doi.org/10.1144/SP427.11

Burtman, V. S., & Molnar, P. H. (1993). Geological and geophysical evidence for deep subduction of continental crust beneath the Pamir. Geological Society of America. https://doi.org/10.1130/SPE281-p1

Cao, K., Wang, G. C., Bernet, M., van der Beek, P., & Zhang, K. X. (2015). Exhumation history of the West Kunlun Mountains, northwestern Tibet: Evidence for a long-lived, rejuvenated orogen. *Earth and Planetary Science Letters*, *432*, 391–403. https://doi.org/10.1016/j.epsl.2015.10.033

Cao, K., Xu, Y. D., Wang, G. C., Zhang, K. X., van der Beek, P., & Wang, C. W. E. T. A. L. (2014). Neogene source-to-sink relations between the Pamir and Tarim Basin: Insights from stratigraphy, detrital zircon geochronology, and whole-rock geochemistry. *The Journal of Geology*, *122*(4), 433–454. https://doi.org/10.1086/676478

Carrapa, B., DeCelles, P. G., Wang, X., Clementz, M. T., Mancin, N., Stoica, M., et al. (2015). Tectono-climatic implications of Eocene Paratethys regression in the Tajik basin of central Asia. *Earth and Planetary Science Letters*, *424*(0), 168–178. https://doi.org/10.1016/j.epsl.2015.05.034

Carrapa, B., Mustapha, F. S., Cosca, M., Gehrels, G., Schoenbohm, L. M., Sobel, E. R., et al. (2014). Multisystem dating of modern river detritus from Tajikistan and China: Implications for crustal evolution and exhumation of the Pamir. *Lithosphere*, *6*(6), 443–455. https://doi.org/10.1130/L360.1

Chapman, J. B., Carrapa, B., Ballato, P., DeCelles, P. G., Worthington, J., Oimahmadov, I., et al. (2017). Intracontinental subduction beneath the Pamir Mountains: Constraints from thermokinematic modeling of shortening in the Tajik fold-and-thrust belt. *GSA Bulletin*, *129*(11-12). https://doi.org/10.1130/B31730.1

Chapman, J. B., Carrapa, B., DeCelles, P. G., Worthington, J., Mancin, N., Cobianchi, M., et al. (2019). The Tajik Basin: A composite record of sedimentary basin evolution in response to tectonics in the Pamir. *Basin Research*, *00*, 1–21. https://doi.org/10.1111/bre.12381

Chapman, J. B., Scoggin, S. H., Kapp, P., Carrapa, B., Ducea, M. N., Worthington, J., et al. (2018). Mesozoic to Cenozoic magmatic history of the Pamir. *Earth and Planetary Science Letters*, *482*(15), 181–192. https://doi.org/10.1016/j.epsl.2017.10.041

Coutand, I., Strecker, M. R., Arrowsmith, J. R., Hilley, G., Thiede, R. C., & Korjenkov, A. (2002). Late Cenozoic tectonic development of the intramontane Alai Valley,(Pamir-Tien Shan region, central Asia): An example of intracontinental deformation due to the Indo-Eurasia collision. *Tectonics*, *21*(6), 1053. https://doi.org/10.1029/2002TC001358

Deenen, M. H., Langereis, C. G., van Hinsbergen, D. J., & Biggin, A. J. (2011). Geomagnetic secular variation and the statistics of palaeomagnetic directions. *Geophysical Journal International*, *186*(2), 509–520. https://doi.org/10.1111/j.1365-246X.2011.05050.x

Gehrels, G. E., Valencia, V. A., & Ruiz, J. (2008). Enhanced precision, accuracy, efficiency, and spatial resolution of U-Pb ages by laser ablation-multicollector-inductively coupled plasma-mass spectrometry. *Geochemistry, Geophysics, Geosystems*, *9*, Q03017. https://doi.org/10.1029/2007GC001805

Harrison, M. T., Grove, M., Mckeegan, K. D., Coath, C. D., Lovera, O. M., & Fort, P. L. (1999). Origin and episodic emplacement of the Manaslu intrusive complex, central Himalaya. *Journal of Petrology*, *40*(1), 3–19. https://doi.org/10.1093/petroj/40.1.3

Jiang, X. D., Li, Z. X., & Li, H. B. (2013). Uplift of the West Kunlun Range, northern Tibetan Plateau, dominated by brittle thickening of the upper crust. *Geology*, *41*(4), 439–442. https://doi.org/10.1130/G33890.1

Kapp, P., & DeCelles, P. G. (2019). Mesozoic–Cenozoic geological evolution of the Himalayan-Tibetan orogen and working tectonic hypotheses. *American Journal of Science*, *319*(3), 159–254. https://doi.org/10.2475/03.2019.01

Kaya, M. Y., Dupont-Nivet, G., Proust, J. N., Roperch, P., Bougeois, L., Meijer, N., et al. (2019). Paleogene evolution and demise of the proto-Paratethys Sea in Central Asia (Tarim and Tajik basins): Role of intensified tectonic activity at ca. 41 Ma. *Basin Research*, *31*(3), 461–486. https://doi.org/10.1111/bre.12330

Kirschvink, J. L. (1980). The least-squares line and plane and the analysis of palaeomagnetic data. *Geophysical Journal of the Royal Astronomical Society*, *62*(3), 699–718. https://doi.org/10.1111/j.1365-246X.1980.tb02601.x

Klocke, M., Voigt, T., Kley, J., Pfeifer, S., Rocktäschel, T., & Keil, S. (2017). Cenozoic evolution of the Pamir and Tien Shan mountains reflected in syntectonic deposits of the Tajik Basin. *Geological Society, London, Special Publications*, *427*(1), 523–564. https://doi.org/10.1144/SP427.7

Liu, D., Li, H., Sun, Z., Cao, Y., Wang, L., Pan, J., et al. (2017). Cenozoic episodic uplift and kinematic evolution between the Pamir and Southwestern Tien Shan. *Tectonophysics*, *712-713*(2017), 438–454. https://doi.org/10.1016/j.tecto.2017.06.009

Liu, X., Sun, H., Miao, Y., Dong, B., & Yin, Z. (2015). Impacts of uplift of northern Tibetan Plateau and formation of Asian inland deserts on regional climate and environment. *Quaternary Science Reviews*, *116*(2015), 1–14. http://doi.org/10.1016/j.quascirev.2015.03.010

McFadden, P. L., & McElhinny, M. W. (1990). Classification of the reversal test in palaeomagnetism. *Geophysical Journal International*, *103*(3), 725–729. https://doi.org/10.1111/j.1365-246X.1990.tb05683.x

Meijer, N., Dupont-Nivet, G., Abels, H. A., Kaya, M. Y., Licht, A., Xiao, M., et al. (2019). Central Asian moisture modulated by proto-Paratethys Sea incursions since the early Eocene. *Earth and Planetary Science Letters*, *510*, 73–84. https://doi.org/10.1016/j.epsl.2018.12.031

Molnar, P., Boos, W. R., & Battisti, D. S. (2010). Orographic controls on climate and paleoclimate of Asia: Thermal and mechanical roles for the Tibetan Plateau. *Annual Review of Earth and Planetary Sciences*, *38*(1), 77–102. https://doi.org/10.1146/annurev-earth-040809-152456

Ogg, J. G., Ogg, G., & Gradstein, F. M. (2016). *A concise geologic time scale: 2016*. Amsterdam: Elsevier.

Popov, S. V., Rögl, F., Rozanov, A. Y., Steininger, F. F., Shcherba, I. G., Kovac, M. (2004). Lithological-Paleogeographic maps of Parathys, *10 Maps Late Eocene to Pliocen*. Stuttgart: Schweizerbart Science Publishers.

Ramstein, G., Fluteau, F., Besse, J., & Joussaume, S. (1997). Effect of orogeny, plate motion and land-sea distribution on Eurasian climate change over the past 30 million years. *Nature*, *386*(6627), 788. https://doi.org/10.1038/386788a0

Robinson, A. C., Yin, A., Manning, C. E., Harrison, T. M., Zhang, S., & Wang, X. (2007). Cenozoic evolution of the eastern Pamir: Implications for strain-accommodation mechanisms at the western end of the Himalayan-Tibetan orogeny. *Geological Society of America Bulletin*, *119*(7-8), 882–896. https://doi.org/10.1130/B25981.1

Rutte, D., Ratschbacher, L., Khan, J., Stübner, K., Hacker, B. R., Stearns, M. A., et al. (2017). Building the Pamir-Tibetan Plateau-Crustal stacking, extensional collapse, and lateral extrusion in the Central Pamir: 2. Timing and rates. *Tectonics*, *36*, 385–419. https://doi.org/10.1002/2016TC004294

Sobel, E. R., & Dumitru, T. A. (1997). Thrusting and exhumation around the margins of the western Tarim basin during the India-Asia collision. *Journal of Geophysical Research*, *102*(B3), 5043–5063. https://doi.org/10.1029/96JB03267

Sun, J., & Jiang, M. (2013). Eocene seawater retreat from the southwest Tarim Basin and implications for early Cenozoic tectonic evolution in the Pamir Plateau. *Tectonophysics*, *588*, 27–38. https://doi.org/10.1016/j.tecto.2012.11.031

Sun, J., Windley, B. F., Zhang, Z., Fu, B., & Li, S. (2016). Diachronous seawater retreat from the southwestern margin of the Tarim Basin in the late Eocene. *Journal of Asian Earth Sciences*, *116*, 222–231. https://doi.org/10.1016/j.jseaes.2015.11.020

Tagami, S., Tagami, T., & Nishimura, S. (1987). Anisotropic etching character of spontaneous fission tracks in zircon. *International Journal of Radiation Applications and Instrumentation. Part D. Nuclear Tracks and Radiation Measurements*, *13*, 275–277. https://doi.org/10.1016/1359-0189(87)90039-2

Tapponnier, P., Xu, Z., Roger, F., Meyer, B., Arnaud, N., Wittlinger, G., & Yang, J. (2001). Oblique stepwise rise and growth of the Tibet Plateau. *Science*, *294*(5547), 1671–1677. https://doi.org/10.1126/science.105978

Tauxe, L. (2009). *Essentials of paleomagnetism*. California: University of California Press.

Vermeesch, P. (2012). On the visualisation of detrital age distributions. *Chemical Geology*, *312-313*, 190–194. https://doi.org/10.1016/j.chemgeo.2012.04.021

Wang, X., Kraatz, B., Meng, J., Carrapa, B., DeCelles, P., Clementz, M., et al. (2016). Central Asian aridification during the late Eocene to early Miocene inferred from preliminary study of shallow marine-eolian sedimentary rocks from northeastern Tajik Basin. *Science China Earth Sciences*, *59*(6), 1242–1257. https://doi.org/10.1007/s11430-016-5282-z

Wang, X., Sun, D., Chen, F., Wang, F., Li, B., Popov, S. V., et al. (2014). Cenozoic paleo-environmental evolution of the Pamir-Tien Shan convergence zone. *Journal of Asian Earth Sciences*, *80*, 84–100. https://doi.org/10.1016/j.jseaes.2013.10.027

Worthington, J. R., Kapp, P., Minaev, V., Chapman, J. B., Mazdab, F. K., Ducea, M. N., et al. (2017). Birth, life, and demise of the Andean-syn-collisional Gissar arc: Late Paleozoic tectono-magmatic-metamorphic evolution of the southwestern Tian Shan, Tajikistan. *Tectonics*, *36*, 1861–1912. https://doi.org/10.1002/2016TC004285

Yang, W., Dupont-Nivet, G., Jolivet, M., Guo, Z., Bougeois, L., Bosboom, R., et al. (2015). Magnetostratigraphic record of the early evolution of the southwestern Tian Shan foreland basin (Ulugqat area), interactions with Pamir indentation and India-Asia collision. *Tectonophysics*, *644-645*, 122–137. https://doi.org/10.1016/j.tecto.2015.01.003

Yin, A. (2010). Cenozoic tectonic evolution of Asia: A preliminary synthesis. *Tectonophysics*, *488*(1), 293–325. https://doi.org/10.1016/j.tecto.2009.06.002

Zachos, J., Pagani, M., Sloan, L., Thomas, E., & Billups, K. (2001). Trends, rhythms, and aberrations in global climate 65 Ma to present. *Science*, *292*(5517), 686–693. https://doi.org/10.1126/science.1059412

Zheng, H., Wei, X., Tada, R., Clift, P. D., Wang, B., Jourdan, F., et al. (2015). Late Oligocene-early Miocene birth of the Taklimakan Desert. *Proceedings of the National Academy of Sciences*, *112*(25), 7662–7667. https://doi.org/10.1073/pnas.1424487112